Broadband precision wavelength meter based on a stepping Fabry–Pérot interferometer

T. J. Scholl,[a] S. J. Rehse, R. A. Holt, and S. D. Rosner
Department of Physics & Astronomy, University of Western Ontario, London, Ontario N6A 3K7, Canada

(Received 26 May 2004; accepted 4 July 2004; published 22 September 2004)

We have constructed a broadband apparatus for wavelength metrology capable of absolute accuracy at a level of better than 2 parts in 10^9. An evacuated plane-parallel Fabry–Pérot interferometer with continuously adjustable mirror separation is used to compare the wavelength of a single-frequency tunable laser with that of an iodine-stabilized HeNe laser used as a wavelength standard. This work details apparatus construction, a thorough investigation of systematic errors, and data analysis. The wavelengths of five Doppler-free $^{130}Te_2$ transitions in the region from 475.6 to 490.8 nm have been measured and are found to be in excellent agreement with previous measurements. In addition, the wavelengths of five previously unmeasured $^{130}Te_2$ transitions spanning the region from 424.9 to 462.3 nm have been determined for use as new reference wavelength standards. © *2004 American Institute of Physics.* [DOI: 10.1063/1.1791871]

I. INTRODUCTION

Wavelength meters based on Michelson or Fizeau interferometers have long been the standard method of wavelength determination for tunable CW dye laser light sources. The wavelength of the "unknown" laser is compared with that of a reference laser by means of fringe counting. The accuracy of these devices is largely limited by the inability to precisely control alignment of the two laser beams in the interferometer.[1] The plane-parallel Fabry–Pérot (FP) interferometer has long been the instrument of choice for precision wavelength measurements on light from incoherent light sources.[2] In recent times FP interferometry has been applied to wavelength comparisons between laser light sources. Petley *et al.*[3] employed a FP locked to an I_2-stabilized HeNe laser to compare the wavelength of a scanning dye laser to that of the HeNe laser. Amin *et al.*[4] used a pressure-scanned FP to compare the wavelength of a dye laser locked to an atomic absorption line to that of an I_2-stabilized HeNe laser. Both experiments measured the Rydberg constant by saturation spectroscopy of the Balmer α line, whose wavelength was already very well known, thus simplifying the task of determining the integer part of the order number.

Sansonetti[5] developed a more general laser wavelength meter in which the FP ring pattern was employed to compare the wavelengths of the unknown and reference lasers, and a traveling Michelson wavelength meter was used to resolve the integer-order-number ambiguity of the FP. Sansonetti's wavelength meter created a pseudo-incoherent light source from the laser beams by scattering from a moving diffuser; this mitigates sensitivity to alignment and collimation of the beams and time-averages over laser speckle. He achieved an accuracy of a few parts in 10^9 in several measurements.[5–7] In the present work we have undertaken a detailed and thorough investigation of the systematics of a new device based on this concept. An important change is the use of a scanning étalon, which allows stepped changes in the mirror spacing during a measurement cycle to diagnose and control systematic errors. We also use a telescope to project the interference pattern, rendering the instrument free of chromatic aberration to a very high degree over a broad spectrum of wavelengths. We have verified its accuracy by measuring the wavelengths of five well-studied Doppler-free transitions in $^{130}Te_2$, and have made precise measurements of five previously unmeasured $^{130}Te_e$ transitions in the 424.9–462.3 nm wavelength range.

The technique of Fabry–Pérot interferometry has been thoroughly discussed by Meissner.[2] The well-known Airy formula gives the intensity pattern of light transmitted through a pair of plane parallel mirrors as

$$I = \frac{T^2/(1-R)^2}{1 + (4R/(1-R)^2)\sin^2(\pi p)}, \tag{1}$$

where T and R are the transmission and reflection coefficients at the mirrors, respectively, and the (generally nonintegral) order number p is the phase difference in one round trip, in units of 2π. For light of vacuum wavelength λ (wave number $\sigma = 1/\lambda$) traveling at an angle of incidence θ to two mirror surfaces separated by a distance t, the order number is given by

$$p = \frac{2t}{\lambda}\cos\,\theta = 2t\sigma\,\cos\,\theta. \tag{2}$$

At the center of the ring pattern ($\theta = 0$), the order number will in general not be integral, but can be written as an integer P plus a fractional part ε

$$p = P + \varepsilon = 2t\sigma. \tag{3}$$

Hence, determination of the integral and fractional parts of the order numbers at the center of the ring pattern for light of unknown wave number σ and known wave number σ_{ref}

[a]Electronic mail: scholl@uwo.ca

(from a reference laser) allows us to determine the unknown wave number quite simply as

$$\sigma = \frac{P + \varepsilon}{P_{\mathrm{ref}} + \varepsilon_{\mathrm{ref}}} \sigma_{\mathrm{ref}}. \tag{4}$$

For the reference laser used in our wavelength meter, σ_{ref} is known absolutely to 2 parts in 10^{10}. With $t = 15$ cm, the integer parts of the order numbers, which are known precisely, are $P_{\mathrm{ref}} \approx 4.74 \times 10^5$ and $P \approx 6.75 \times 10^5$ (for $\sigma \approx 22\,500\ \mathrm{cm}^{-1}$). Measuring the ring patterns determines ε and $\varepsilon_{\mathrm{ref}}$ to 5×10^{-4}, and thus the absolute accuracy of the method is about 1 part in 10^9.

The fractional order numbers are determined by observing a slice through the Airy ring pattern with a silicon-diode array, alternately exposing the instrument to light from the unknown and reference lasers. Although it would appear from the formula above that it is not necessary to know the mirror separation t, in fact this must be measured very precisely in order to deduce the integer parts of the order numbers. We accomplish this by the "method of exact fractions,"[8,9] using a traveling Michelson wavelength meter with an absolute accuracy of better than 1×10^{-7}. Once t is known to a precision of ≈ 0.3 ppm, P_{ref} and P can be obtained from $\varepsilon_{\mathrm{ref}}$ and ε (measured from the ring pattern), σ (measured approximately with the Michelson wavelength meter), and σ_{ref}.

A small but significant correction at our level of accuracy arises from the wave number dependence of the phase shift upon reflection from the aluminum mirrors, which has not been included in the formulas above. The resulting correction to the order number is less than 5×10^{-3} over the wavelength region of interest, and is determined to a fractional accuracy of 10% by the "method of virtual mirrors,"[2,10] in which measurements are made with different mirror spacings.

II. APPARATUS

A. Interferometer

Figure 1 is a schematic diagram showing the experimental components and the light paths between them. The laser beams from the frequency-offset-locked HeNe laser and a CW dye laser are separately expanded by lenses. Computer-controlled electromechanical shutters in the path of each laser beam are used to select light from either laser for individual analysis by the Fabry–Pérot interferometer. The paths of the two laser beams are combined by a polarizing beam-splitter cube. An expanded laser beam is focused by a 100 mm focal-length cylindrical lens to form a horizontal line source on a spinning plastic wheel for illumination of the interferometer. The downstream face of the plastic wheel is roughened to scatter the transmitted laser beam over a broad range of angles and to destroy its coherence, thereby removing the speckle pattern on the interference rings, which would be a source of noise. The scattered laser light is collimated by an 80 mm focal-length achromatic lens and masked by a 33 mm diam aperture before entering the FP vacuum enclosure.

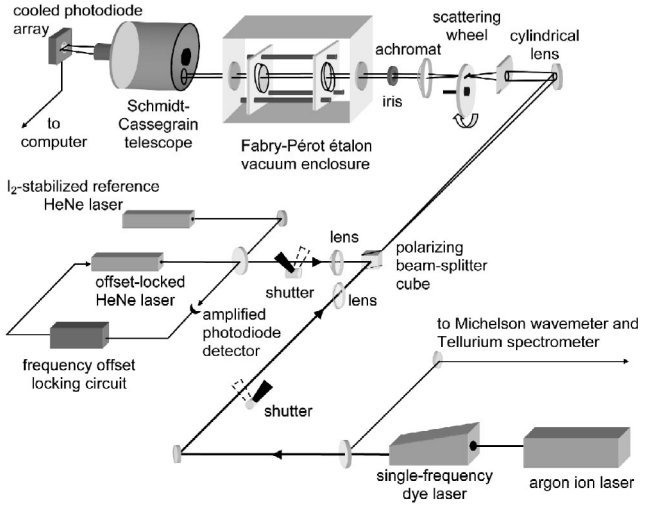

FIG. 1. Schematic apparatus diagram. A HeNe laser offset-locked to an I_2-stabilized HeNe laser serves as the reference for wavelength determination of a CW dye laser locked to a saturated absorption line in Te_2. A Fabry–Pérot étalon is illuminated separately by light from these two lasers and the resulting transmitted interference ring patterns are measured on a linear photodiode array (PDA).

The plane-parallel FP étalon (Burleigh Model RC-110) is housed in a vacuum enclosure to eliminate corrections for the index of refraction of air. The vacuum is maintained below 30 mbar by a roughing pump isolated by a molecular sieve filter to prevent contamination of the étalon mirrors. The 50.8 mm diam vacuum windows are anti-reflection coated BK-7 glass plates, flat to $\lambda/10$ and parallel to 5 arc s. The matched $\lambda/200$ étalon mirrors are 50.8 mm diam Spectrosil-B blanks possessing a flatness finesse of 100. The reflectivity of the aluminum coatings is 85% at 632.8 nm, resulting in a reflectivity finesse of 19.3. Bare aluminum is chosen for the reflecting surfaces since its reflectivity is broadband and phase shifts due to reflections from these surfaces are small and vary smoothly with wavelength.[11,12] Observed finesses vary from a maximum of 16 at the reference wavelength to ≈ 12 at 420 nm. These modest finesses spread the intensity of an interference fringe projected onto the photodiode array detector over at least 5 pixels for accurate determination of fringe positions to better than a single pixel width. The uncoated sides of the étalon mirrors are wedged by 10 arc minutes; the wedge angles of the étalon plates are oriented at 180° with respect to each other, with the apexes of the "prisms" up and down. These wedge angles eliminate formation of additional étalons from these faces, but weak back reflections from the uncoated sides produce faint secondary copies of the FP ring pattern above and below the main pattern. The intensity of the secondary patterns where they overlap the primary pattern is essentially zero due to the line source illumination at the scattering wheel.

Coarse alignment of the étalon mirrors is accomplished by fine-pitch mechanical screws. The ultimate alignment of the étalon is made in vacuum by three piezoelectric crystal (PZT) adjusters while simultaneously monitoring the measured finesse from an analysis of the interference pattern. In addition to these alignment PZTs, 3 stacks of matched PZTs can be used to scan the étalon separation over a distance of

2 μm corresponding to $\Delta P_{\mathrm{ref}} \approx 6$. This capability has proved to be invaluable for understanding experimental systematics, and is a significant departure from previous FP-based wavelength meters where the étalon spacings are static (except for slowly varying drifts). Fabrication of the étalon assembly, with the exception of the PZT material, is almost entirely from Super Invar (coefficient of linear expansion $\alpha \leqslant 0.36 \times 10^{-6}\ ^{\circ}\mathrm{C}^{-1}$). The mirror mount holding the PZT-actuated étalon mirror is clamped to three Super Invar rods; it may be translated along the rods and reclamped, permitting a choice of the mirror spacing from less than 0.1 cm up to 15 cm. Remounting the scanning mirror backwards and reversing this mirror mount permits spacings up to 22.5 cm, which were useful in determining the mirror phase shifts. After evacuation of the étalon housing and thermal stabilization of the étalon, drifts in the mirror spacing of approximately 1 nm per hour or less were observed for a spacing of 15 cm.

Transmitted light emerging from the FP vacuum enclosure is focused onto the photodiode array (PDA) by a 2000 mm focal-length Schmidt-Cassegrain telescope, or a pair of achromatic lenses in the case of small values of the separation t of the étalon mirrors. An off-center portion of the 200 mm entrance aperture of the telescope is used to collect the light. With the exception of the Schmidt plate, the telescope is all reflecting and thus nearly free of chromatic aberration. The telescope has the further advantage that its optical design results in a more compact apparatus compared to that employing an achromatic lens of comparable focal length. Mounting of the PDA onto the telescope is rather straightforward given the standard threaded mount found on the telescope. This results in an optical system that is easily aligned on the ring pattern by translating the telescope and PDA as a single unit, and is readily focused by the manual control that translates the primary telescope mirror. For $t < 4$ cm, a combination of two achromatic lenses producing a 666 mm focal length replaces the telescope to produce an interference pattern with 10–15 rings on the PDA.

A slice along a diameter of the projected ring pattern is detected by a linear PDA. The EG&G Reticon K-Series chip consists of 1024 silicon photodiodes on 25 μm centers, each with a height of 250 μm. The PDA has a quartz window and is cooled to 5 °C to reduce dark noise, permitting longer integration times. The light intensity recorded by individual pixels is digitized at a rate of 195 kHz by a computer data-acquisition board, with complete patterns acquired every 13.5 ms. Typically, 10 individual ring patterns are acquired and averaged for display and analysis. Data acquired with the PDA darkened are used for background subtraction. A full measurement cycle, including acquisition and analysis of one averaged ring pattern from each laser, is completed at a rate of approximately 1 Hz.

The reference wavelength used in this work is generated by a Winters Electro-Optics Inc. Model 100 I_2-stabilized HeNe laser whose frequency is known to a few parts in 10^{11}. To provide a reference beam of increased intensity without frequency modulation, a single-frequency HeNe laser (Research Electro-Optics Inc. Model LTRP−0051-BW-NS) housed in a pressure-stabilized Invar cavity is frequency-offset-locked to the reference laser, yielding 900 μW of power. The frequency offset ($\approx$13 MHz) is directly measured by a frequency counter monitoring the beat frequency of a portion of the offset-locked laser output combined with that of the I_2-stabilized HeNe laser on an amplified photodiode (New Focus Model 1801). The uncertainty in the beat frequency of $\approx$0.1 MHz leads to an accuracy of $\approx 2 \times 10^{-10}$ for our reference wavelength.

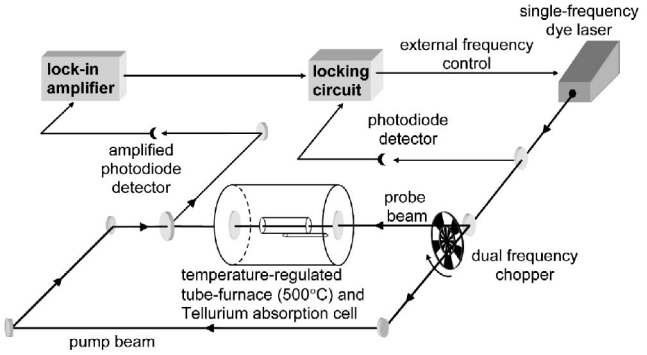

FIG. 2. Saturated absorption spectrometer. Light from a dye laser is split into separate pump and probe beams, modulated by a dual frequency chopper, and overlapped in a $^{130}Te_2$ cell heated to 500 °C in a temperature-regulated furnace. The resulting saturated-absorption signal is used to lock the dye laser frequency to the side of the absorption line.

B. Tellurium saturated-absorption spectrometer

A schematic of the intermodulation[13] saturated-absorption spectrometer is shown in Fig. 2. Laser light from the dye laser using Stilbene 420 or Coumarin 480 is split into a pump beam and a weaker probe beam ($I_{\mathrm{pump}}/I_{\mathrm{probe}} \approx 10$). A dual-frequency chopper modulates the pump and probe beam intensities at 3.0 and 2.5 kHz, respectively, and supplies a reference signal at 5.5 kHz. Mirrors reflect the two beams to be collinear and overlapped as they traverse the tellurium absorption cell in opposite directions. A portion of the probe beam after transmission through the cell is sampled with a beam splitter, detected by an amplified photodiode, and phase detected at the 5.5 kHz sum frequency by a lock-in amplifier.

The absorption cell is an evacuated 7.5 cm-long, 2.5 cm diam sealed quartz cylinder containing a small amount of ^{130}Te. A tube furnace heats the cell to produce a calculated Te_2 vapor pressure[14] of 0.91 mbar at 502 °C. The furnace has quartz windows on either side to reduce temperature gradients while permitting transmission of the laser beams. The cell is centered in the furnace, while its cold arm, which is bent to be parallel to the axis of the cell, extends 5 cm beyond the cell window into a region of lower temperature nearer a furnace window. The cell body temperature varies from 520 °C near its center to approximately 515 °C at its windows. A temperature controller deriving its input from a type-K thermocouple attached to the cold finger regulates the temperature to within 3 °C of the set point with an absolute measurement accuracy of better than 2 °C. We estimate the total uncertainty in determining the coldest point of the Te_2 cell to be an additional 5 °C, yielding an overall uncertainty in the cold-point temperature measurement of 6 °C. The corresponding vapor pressure of Te_2 and its uncertainty

is 0.91(13) mbar. The single-pass absorption for the Te_2 vapor at 502 °C is 23(2)% for the Doppler-limited line at 20 564.385 cm^{-1}, in agreement with other work.[7] For the same cell temperature, the single pass absorption at 22 634.330 cm^{-1} is 85(3)%.

The frequency of the tunable dye laser is stabilized by locking it to the side of a saturated absorption line using the DC ratio method. In this method, the output of the lock-in amplifier is analog-divided by a laser power signal to remove small (<2% peak-to-peak) dye-laser intensity fluctuations, and the output is compared to a reference voltage. The voltage difference generates an error signal, which is fed back into the dye laser's external frequency input. Assuming symmetric line profiles, wavelength measurements were made with the dye laser locked alternately on both sides of the saturated absorption line at the same fractional absorption and averaged. A fitting analysis of the line shapes with symmetric and asymmetric Lorentzian profiles indicates that, with the present signal-to-noise (S/N) ratio, no asymmetries that could shift the measured line center by more than 200 kHz can be detected. The line shapes have full widths at half maximum (FWHM) of 15–25 MHz. Significant power broadening of 5–7 MHz was observed for several strong lines at higher pump powers (>50 mW). No statistically significant shifts in the measured wave numbers were observed for lock-points varying between 25% and 75% of maximum saturated absorption.

For measurements spanning the wavelength region from 424.9 to 462.3 nm, the output power from the dye laser ranged from 75 to 350 mW for Stilbene 420 dye pumped with 4.75 W of ultraviolet light from an Ar^+ pump laser. About 60% of that power was required for saturated absorption measurements, producing line shapes with excellent S/N ratios of ≈75. The typical FP input power was 1.5 mW for wavelength measurements in the range 420–465 nm, where the responsivity of the PDA is lower by a factor of ≈2.5 compared to that at the reference wavelength. The relative intensity of the two laser beams and the extent of their expansions along the horizontal plane were adjusted to produce ring patterns with similar intensity envelope distributions for both lasers. The majority of the remaining light (≈25 mW) was directed to a Michelson wavelength meter. In the 475.6–490.8 nm region, Coumarin 480 dye pumped by 3.0 W of ultraviolet light produced only 35–85 mW of output power. The increased laser intensity fluctuations as well as reduced Te_2 absorptions in this spectral window resulted in S/N ratios of less than 10 in the observed saturated-absorption signals.

C. Michelson wavelength meter

The Michelson wavelength meter is based on a triangular design by Hall.[15] The reference laser is a polarization-stabilized HeNe. A small NIST-traceable "weather station" monitors temperature, pressure and humidity, from which a correction for the index of refraction of air is calculated. With approximately 45 cm of travel and ×20 fringe multiplication of the HeNe reference fringes, it achieves an absolute accuracy of $\leqslant 1\times10^{-7}$. This level of accuracy is necessary and sufficient for an accurate determination of the étalon spacing by the method of exact fractions.[8,9] Our implementation of this method utilizes measurements of the dye laser wave number and the fractional order number at the center of the ring pattern in the FP étalon for 8 wavelengths geometrically spaced over a 1000 cm^{-1} span; details of the method are given in the Appendix. In addition, the fractional order number of the light from the offset-locked HeNe laser, ε_{ref}, is measured. Together these data are analyzed for unambiguous determination of the spacing of the étalon mirrors to better than 1 nm for subsequent calculation of the integer part of the order number at the center of the ring pattern. This procedure is necessary only once a day at the start of data acquisition due to the very slow drift of the étalon spacing. The Michelson wavelength meter is also used initially to set the wavelength of the dye laser for a particular Doppler-free transition to within 0.002 cm^{-1}.

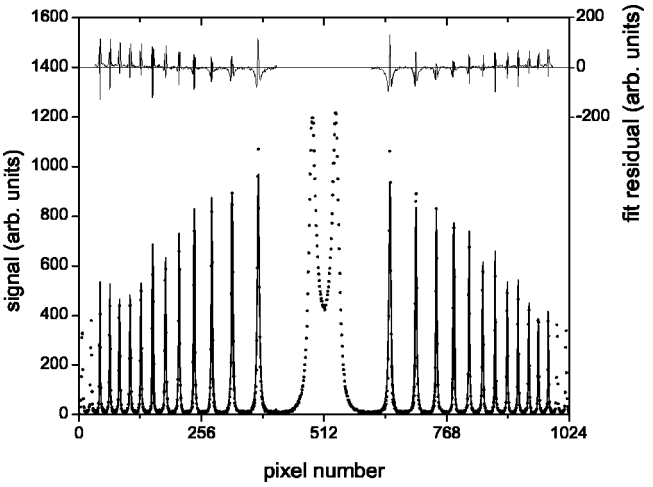

FIG. 3. A typical Fabry–Pérot interference pattern for 632.8 nm laser light (dots) and a fit to a product of an Airy function and a Gaussian intensity envelope (line). The upper curve shows the residuals from the fit. The fractional order number is 0.0334(4) and the finesse is 14.2. The pattern is the average of 10 scans of the PDA, each requiring 13.5 ms.

III. RING PATTERN ANALYSIS

As discussed in the Introduction, it is necessary to determine the fractional part of the order number at the center of the ring pattern, ε, to a relative precision of 5×10^{-4} to achieve a precision of 1×10^{-9} in the measured wave number. To investigate possible systematic errors in the determination of ε, the ring patterns were analyzed by a standard nonlinear least-squares (NLLS) fit to a modified Airy pattern ("Airy method") and also by the usual analysis method involving a plot of ring number versus the square of the ring radius ("rings method").[2]

A. Airy method

Figure 3 shows a typical ring pattern recorded by the PDA, the results of a NLLS fit to it, and the subsequent residuals. The fitting model for intensity I as a function of position x on the PDA is given by a Gaussian intensity envelope with peak intensity I_0, center location x_0, and FWHM $2w\sqrt{\ln 2}$, times an Airy function $A(x)$, plus a constant background B

$$I(x) = I_0 e^{-(x-x_0)^2/w^2} A(x) + B. \tag{5}$$

The Airy function, approximated for small angles of incidence on the étalon, is given by

$$A(x) = \frac{1}{1 + f \sin^2\{\pi[\varepsilon - (x-x_c)^2/s]\}}, \tag{6}$$

where f is a parameter related to the finesse F according to $f=(2F/\pi)^2$, ε is the fractional part of the order number at the center of the ring pattern, x_c, and s is a parameter related to the focal length f of the projection system and the integer part of the order number at the center of the pattern, P, according to $s=2f^2/P$. (Note that x_c, the center of the interference pattern, is close to, but not necessarily exactly coincident with, the center of the intensity envelope, x_0.) In total eight parameters, $I_0, x_0\ w, B, f, x_c, s$ and, most importantly, ε, are adjusted in the NLLS fit.

B. Rings method

A ring is defined by the locus of points at which the Airy function reaches a local maximum. For rays with nearly normal incidence on the étalon, it can be shown from Eq. (6) that the radius of the j^{th} ring, $r_j = x_j - x_c$, where x_j is the location of the local maximum, satisfies

$$r_j^2 = s(j - 1 + \varepsilon). \tag{7}$$

Thus a linear plot of r_j^2 vs j yields ε as $\varepsilon = 1 +$ intercept/slope. The individual x_j are determined by fitting a function derived as an approximation to Eq. (6) which is valid in the vicinity of a ring peak when $2F/\pi \gg 1$. It is multiplied by the Gaussian envelope function described above to correct for the nonuniform laser intensity across the ring peak

$$I(x) = I_0 e^{-(x-x_0)^2/w^2} \frac{1}{1 + \kappa_j (x_j^2 - x^2)^2} + B. \tag{8}$$

Here $\kappa_j \approx 1/(W_j r_j)^2$ where W_j is the FWHM of the ring, and all other parameters are as defined for Eq. (6). Equation (8) contains the asymmetry of the ring peaks, which decreases with increasing ring radius.

The Gaussian-envelope parameters I_0, x_0, w and the background B are determined by modeling the entire ring pattern as in the "Airy method". Except for I_0, they are fixed during the fit of a single ring peak.

IV. MIRROR PHASE SHIFT CORRECTION

The formula for the "unknown" wave number given in Eq. (4) does not include the effect of the phase change upon reflection from the Al mirrors. It is convenient to include the phase change at the reference wavelength in an effective mirror separation, t, and introduce a wave-number-dependent *relative* phase correction $\delta(\sigma)$ which is zero at σ_{ref}. Hence Eq. (3) becomes

$$\sigma = [P + \varepsilon + \delta(\sigma)]/2t. \tag{9}$$

The standard method of determining the phase correction is to measure the same wave number at two mirror separations,[2,10] sometimes referred to as the "method of virtual mirrors." It can be seen from Eqs. (3) and (9) that the wave number measured without taking the phase correction into account, σ_{meas}, is related to the true wave number σ by

$$\sigma_{\text{meas}} = \sigma - \frac{\delta(\sigma)}{2t}, \tag{10}$$

and thus a plot of σ_{meas} vs $1/2t$ yields the true wave number as its intercept and the phase shift as the negative of its slope. By taking measurements at *more* than two spacings, we can test for possible systematic errors.

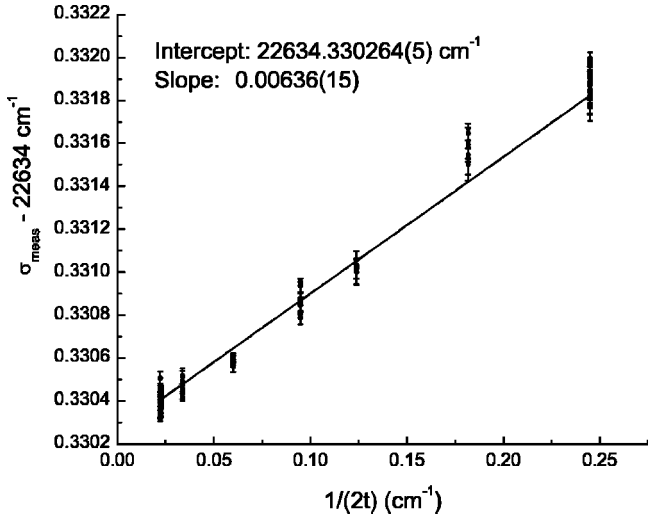

FIG. 4. Measured wave number, σ_{meas}, for the saturated-absorption line at 22 634.330 cm^{-1} versus $1/(2t)$, where t is the étalon spacing. The phase correction, $\delta(\sigma)$, at this wave number is equal to the negative of the slope and the phase-corrected wave number is the intercept.

Doppler-free $^{130}\text{Te}_2$ transitions with $\sigma < 21\,626\ \text{cm}^{-1}$ were measured at four different étalon spacings ranging from 2.76 to 22.54 cm. The remaining transitions were measured at 7 spacings spanning essentially the same range. Measurements of the saturated absorption transition at 22 634.330 cm^{-1} as a function of $1/(2t)$ are shown in Fig. 4, illustrating typical results. There are 77 line-center measurements in total, with 47 of those made at the maximum spacing. The linear fit gives $\delta = -0.006\,36(15)$ and $\sigma = 22\,634.330\,264(5)$. Uncertainties for the parameters of the linear fit have been scaled by the square root of the reduced chi-squared ($\sqrt{\chi^2_{\text{reduced}}} \approx 1.7$).

Because $\delta(\sigma)$ is a smoothly varying function,[11,12] a more accurate value can be obtained by fitting the data for our whole range of wavelengths to a single function of σ. The statistical information is only sufficient for a linear fit. (Note that the dependence over the full range from our region to 632.8 nm is *not* linear and thus we do not constrain the intercept.) The dependence of δ on σ over the spectral region of interest is shown in Fig. 5. Uncertainties for the parameters of the linear fit have been scaled by $\sqrt{\chi^2_{\text{reduced}}} \approx 2.1$. The rms residual from the fit to these data is 0.000 43 and the maximum residual is 0.000 84. For an étalon spacing of 22.5 cm, choosing $\delta = -0.004\,32(43)$ at $\sigma = 21\,615\ \text{cm}^{-1}$ (the center of the wave number range) yields a phase correction to σ of −2.9(3) MHz, or a fractional correction of $4.4(4) \times 10^{-9}$. Thus the phase correction is essential, but its uncertainty contributes only about 4 parts in 10^{10} to the error budget.

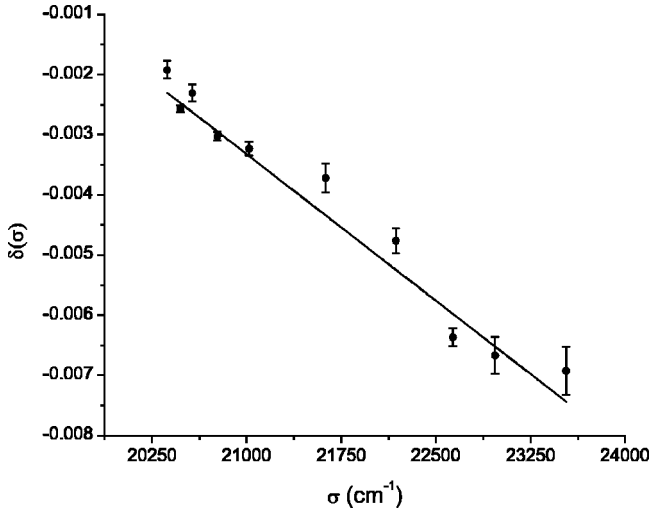

FIG. 5. The wave-number-dependent phase correction $\delta(\sigma)$ arising from reflections in the Fabry–Pérot étalon has been measured at 10 different wave numbers (see Fig. 4 for a typical measurement) and analyzed with a linear fit.

V. SYSTEMATIC ERROR INVESTIGATION

Comparison of the dye laser wave number computed from fractional orders derived by these two independent methods serves as a check for computational and systematic errors in analysis.

A. Computer simulations

Modified Airy patterns were computer-simulated under a variety of assumptions in order to evaluate possible causes of systematic error in values of ε, and hence in the final wave number σ. The main conclusions are as follows:

(1) The value of ε is not sensitive either to creating a pattern with one envelope function (e.g., Gaussian) and analyzing it with another (e.g., triangular), or moderately shifting the analysis envelope relative to the creation envelope.
(2) The value of ε is not sensitive to integrating over pixel height. This was determined by including this integration in the simulation of a pattern with a known value of ε, but then analyzing that pattern for ε using a model that assumes zero pixel height. The ability to ignore this integration in the analysis of the Airy pattern dramatically sped up data acquisition.
(3) Ignoring the central region of the Airy pattern in the analysis produces closer agreement between the two methods of analysis. When ε is near 0 or 1, there is a broad central "bull's eye" whose shape is quite sensitive to the envelope function but contributes very little to the knowledge of ε, and for other values of ε, the central region contains only noise. In all our data analysis the central region is, therefore, omitted.
(4) In the rings method, fitting the individual peaks with the function of Eq. (8) gives better results than a symmetric function such as a parabola or a Gaussian. The use of Eq. (8) produces fractional differences between input and analyzed values of σ at a level of 2×10^{-10} (comparable to the "Airy method"), compared to typically $10\times$ worse for the symmetric functions. These tests were done by averaging up to 100 simulations with random noise.

The differential refraction of the unknown and reference interference patterns by the wedged substrate of the final étalon mirror was examined theoretically and found to be inconsequential at our level of precision.

B. Experimental tests

The simulations were complemented by a number of experimental tests for systematic problems. One of the most important relies on the ability to scan the étalon spacing systematically using the PZT actuators. The addition of systematic variation of the étalon spacing represents a marked improvement over previous wavelength meters employing a fixed-spacing étalon that required a series of wavelength measurements acquired over several days as the étalon spacing slowly drifts to build a set of measurements spanning significantly different values of ε for both the reference and unknown lasers.

With the dye laser frequency-locked to the side of a saturated absorption feature, its wave number is repeatedly measured as the étalon spacing is stepped through a small change in distance. The initial étalon spacing is determined by the method of exact fractions. After a measurement of the dye laser wave number, the computer reduces the étalon spacing by a small amount ($\Delta t=6.3$ nm) corresponding to $\Delta\varepsilon_{\mathrm{ref}}=0.02$, computes a trial value for the new spacing, and performs another measurement. This is repeated 50 times until the mirror completes a full cycle of translation corresponding to $\Delta\varepsilon_{\mathrm{ref}}=1$. A typical standard deviation for these 50 measurements, which is used as the measurement error, is less than 1 MHz. The laser wave number is then re-measured at the opposite lock point of the saturated-absorption line shape and the two results are averaged to produce a single determination of the transition wave number.

This important diagnostic procedure uncovered a subtle systematic error which we were able to eliminate by changing the procedure used to focus the ring pattern, as well as the projection lens used at small mirror spacings. Repeated wave number measurements of the dye laser locked to a saturated absorption line were made as the étalon spacing was scanned over one order of interference at 632.8 nm. A plot of the measured wave number versus HeNe fractional order, at a small mirror spacing ($t=6.7$ mm), shown in Fig. 6, illustrates obvious discontinuities. It is apparent from Eq. (4) that at shorter spacings, where the integer part of the order number is smaller, this effect is magnified. These discontinuities arise at the two spacings where either ε or $\varepsilon_{\mathrm{ref}}$ crosses 0 or 1. It is precisely at these two points that the analysis procedure for determination of ε from the ring pattern ignores another innermost ring in order to exclude the central section as described above. Since the measured wave number must be independent of the étalon spacing as well as the portion of the Airy pattern we choose to analyze, these discontinuities suggested to us that there might be a systematic deviation of the measured ring pattern from the theoret-

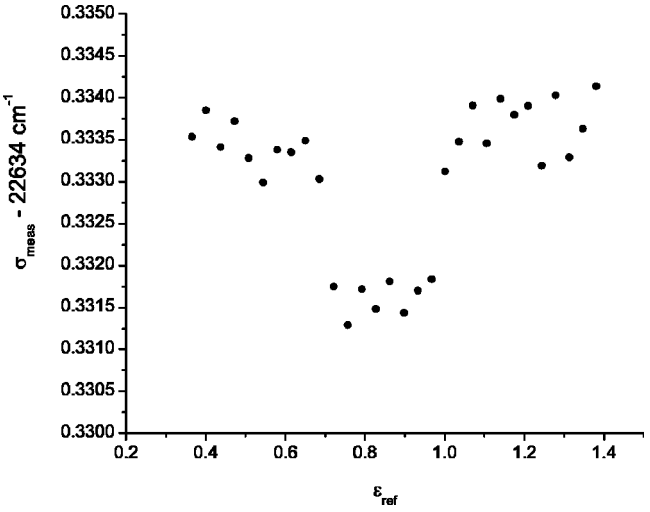

FIG. 6. Measured wave number, σ_{meas}, vs fractional order number ε_{ref}. A systematic effect is clearly evident in the measured wave number of a $^{130}Te_2$ saturated absorption line as the étalon spacing is varied through one order of interference at 632.8 nm. These discontinuities, which arise when either ε or ε_{ref} crosses 0 or 1, are evidence of deviation of the measured ring pattern from an Airy pattern. This problem was eliminated by a new focusing procedure and a more achromatic projection system.

ical Airy pattern (modified by the intensity envelope function).

We then improved our data acquisition program to display in real time the residuals from the fit to Eq. (7) in the rings method, and indeed observed a nonrandom pattern. We found that we could remove this effect from either the HeNe pattern or the dye-laser pattern, but not both at the same time, by means of a small adjustment of the focus of the projection lens (1 to 2 mm), which consisted of a 500 mm focal-length achromatic lens in the case of the small mirror spacings. This suggested that the observed effect was due to chromatic aberration. We substituted a combination of two different achromats with an effective focal length of 666 mm to improve the compensation for this effect. The Schmidt–Cassegrain telescope used to project the ring patterns onto the PDA for the longest étalon spacings exhibited essentially zero chromatic aberration.

It was then necessary to find a new criterion for positioning the PDA at the focal plane of the projection optics. Our original method was to choose a PDA position that maximized the observed finesse. We subsequently found that the optimum focusing condition is obtained by monitoring plots of the residuals from the rings method linear regression, as well as observing the fringe pattern and a numerical display of the finesse for both reference and "unknown" lasers. Small changes from the optimum focusing distance (<5 mm for the 666 mm-focal-length achromat) produce obvious systematic deviations from zero in these residual plots, which tend to be similar for both lasers. The PDA position is changed until the residuals are minimized and the plots are flat for both lasers, and the observed finesses, adjusted by the mirror PZTs, are at a maximum. Data are always taken with a series of values of ε_{ref} corresponding to an order change of 1 to check that discontinuities in the plot of measured wave number versus ε have been eliminated.

Another potential source of systematic error is the recording of a slice of the Airy pattern that is not along a diameter. To ensure that the PDA is aligned with the center of the ring pattern, the PDA is translated in the vertical direction while simultaneously monitoring ε and looking for a maximum. Repetition of this process by different individuals leads to a scatter in the measured wave number of no greater than 0.2 MHz, and is implicitly included in the error budget as part of the item "reproducibility of results" (see below). The position of the incoming laser light on the scattering wheel is then re-optimized to ensure maximum intensity recorded on the PDA. (Although the interference pattern depends only on the projection lens, the intensity envelope depends also on the collimating lens and the source location.) This procedure is then repeated several times. The PDA is also translated horizontally so that the observed ring pattern, as reported by the analysis software, is centered on the array.

VI. RESULTS AND DISCUSSION

A series of identical measurements of a given Doppler-free saturated absorption line acquired over a few minutes reveals a statistical scatter that is much less than 1 MHz. Repetition of measurements of that transition on subsequent days or after major changes of the alignment of the optics produces small systematic shifts in the measured wave number. The probable sources of these shifts are distortions of the observed ring patterns due to changes in alignment of the PDA with respect to the center of the pattern, the focusing of the final projecting optics onto the PDA, aberrations in these focusing optics, or even changes in adjustment of the étalon parallelism. Repeated measurements of transition wave numbers taken at the longest étalon spacing over several weeks have a standard deviation of 0.98 MHz, which we adopt as our estimate of the reproducibility of the measurements.

Typical pressure shifts for saturated absorption line centers in this wavelength region and temperature are ≈ 0.75 MHz/mbar.[16–18] For a 0.13 mbar uncertainty in the Te_2-cell pressure arising from the 6 °C temperature uncertainty, the uncertainty in the pressure shift should be $\leqslant 0.1$ MHz. Since the pressure shift varies with σ, a conservative estimate of the uncertainty due to pressure shifts is 0.3 MHz. Uncertainties in the offset-lock frequency are less than 0.2 MHz. Other uncertainties such as the frequency of the reference laser and dispersion in the index of refraction of residual gas in the evacuated FP étalon are negligible at this level of precision. Assuming that the uncertainties in determination of the phase dispersion correction (0.3 MHz), measurement reproducibility (0.98 MHz), pressure shifts of absorption line centers (0.3 MHz), line shape asymmetry (0.2 MHz) and offset-lock frequency (0.2 MHz) are independent, they have been added in quadrature to obtain a 1.1 MHz or 0.000 037 cm^{-1} overall estimate for the uncertainty in the wave number determination of these $^{130}Te_2$ transitions. The error budget is summarized in Table I.

Measurements of $^{130}Te_2$ transitions spanning the spectral region from 20 369 to 23 531 cm^{-1}, using the longest étalon spacing, have been corrected for the reflective phase shifts in

TABLE I. Measurement uncertainties. See text for further explanation.

Source of uncertainty	Uncertainty (MHz)
Residual gas index of refraction dispersion	negligible
Reference frequency	negligible
Offset-lock frequency	0.20
Absorption line shape asymmetry	0.20
Pressure shifts	0.30
Phase-shift determination	0.30
Reproducibility of results (statistical)	0.98
Overall total (quadrature)	1.10

the étalon mirror coatings with the values of $\delta(\sigma)$ from the fit shown in Fig. 5. These results and previous measurements[7,17,19] are summarized in Table II. The agreement with previous high-accuracy work of similar uncertainty is excellent, supporting the assertion that these measurements of Doppler-free saturated-absorption transitions in tellurium are accurate standards at the ±1 MHz level. We are in the process of increasing the number of measured transitions in the spectral range from 21 500 to 23 750 cm^{-1} for $^{130}Te_2$, where no other convenient frequency standards exist at this level of precision. We are also planning to incorporate frequency-modulation spectroscopy as a replacement for the DC ratio method of frequency-locking the dye laser to the saturated $^{130}Te_2$ features. This should improve the measurement scatter and increase our rate of data acquisition significantly. We also intend to extend the wavelength measurement range of the instrument into the infrared region. The only necessary change involves the replacement of the silicon PDA with an InGaAs array.

ACKNOWLEDGMENTS

This work has been funded by the Canadian Institute for Photonic Innovations and by the Natural Sciences and Engineering Research Council of Canada. The authors would like to thank Dr. Alan Madej of the National Research Council of Canada's Institute for National Measurement Standards for assistance in transferring laser frequency-offset-locking technology to our laboratory and Dr. Craig J. Sansonetti of the National Institute of Standards and Technology, Gaithersburg Md., for many stimulating and encouraging conversations. Finally, the authors would like to thank Mr. Harry Chen for technical assistance with electronics and Mr. Grant Wu and Mr. Ryan Rivest for early development work on our Michelson wavelength meter and the saturation-spectroscopy apparatus.

APPENDIX: METHOD OF EXACT FRACTIONS

The "method of exact fractions"[8,9] determines the integer part of the order number, P, and a precise value of the mirror spacing, t, by making use of determinations of the fractional part, ε, for at least two reasonably well-known wave numbers. From Eq. (4) we see that the order numbers must satisfy

$$\frac{P_2+\varepsilon_2}{P_1+\varepsilon_1}=\frac{\sigma_2}{\sigma_1}. \tag{A1}$$

Using an approximate value of t, known values of σ_1 and σ_2, and the measured values of ε_1 and ε_2, we obtain initial guesses for P_1 and P_2. A search of integer values for the latter then determines the pair that make the fractions agree.

With the advent of tunable CW lasers, it makes sense to inquire if there is an efficient way to choose $\sigma_1,\sigma_2,\ldots$ to maximize the efficiency of this procedure, given that arbitrary wave numbers can be generated and measured to $\leqslant 10^{-7}$ absolute accuracy with a traveling Michelson wavelength meter. Indeed, we have found a method in which *no search is necessary*. Our idea is to choose wave numbers separated by intervals that form a geometric progression

$$\sigma_j-\sigma_{j-1}=r(\sigma_{j-1}-\sigma_{j-2}). \tag{A2}$$

The first interval is chosen to be small enough to be conveniently *counted*, for example $\sigma_1-\sigma_0=1\ cm^{-1}$, corresponding to $P_1-P_0=30$ for a 1 GHz-FSR étalon. Then, at each step j of the procedure we determine the difference of integer orders *exactly* by using the approximate t from the *previous* step,

TABLE II. Saturated absorption measurements of $^{130}Te_2$. Measurements of wave numbers (cm^{-1}) of 10 transitions in $^{130}Te_2$, spanning the region from 425 to 491 nm are compared with existing high-accuracy work.

This work	Gillaspy and Sansonetti (Ref. 7)	McIntyre and Hänsch (Ref. 17)	Barwood *et al.* (Ref. 19)
20 369.513 701(37)	20 369.513 706(44)		
20 476.871 022(37)	20 476.871 017(30)	20 476.871 063(20)	20 476.871 033(16)
20 569.705 514(37)	20 569.705 510(44)		
20 769.195 166(37)	20 769.195 160(44)		
21 020.718 476(37)	21 020.718 447(44)		
21 626.668 960(37)			
22 184.304 882(37)			
22 634.330 275(37)			
22 970.191 921(37)			
23 530.779 797(37)			

$$P_j - P_{j-1} = \mathrm{nint}(2t_{j-1}(\sigma_j - \sigma_{j-1}) - (\varepsilon_j - \varepsilon_{j-1})), \tag{A3}$$

where "nint" stands for nearest integer, and we compute a more accurate value of the spacing, t_j, from Eq. (3)

$$t_j = \frac{(P_j - P_{j-1}) + (\varepsilon_j - \varepsilon_{j-1})}{2(\sigma_j - \sigma_{j-1})}. \tag{A4}$$

In order for this procedure to succeed, the calculated uncertainty in the difference of integer parts, Δ_P, must be much less than 1 at each step, so that the true difference can be determined unambiguously. A standard error propagation, in which the uncertainty in the wave numbers measured by the Michelson wavelength meter, Δ_σ, dominates over that in the FP fractional orders, Δ_ε, shows that the geometric ratio must be chosen to satisfy

$$r < \sqrt{(\Delta_P \cdot 1\ \mathrm{cm}^{-1}/30\sqrt{2}\Delta_\sigma)^2 - 1}. \tag{A5}$$

For $\Delta_P = 0.2$ and $\Delta_\sigma = 0.001\ \mathrm{cm}^{-1}$, we find $r < 4.6$. Thus, for example, 6 geometrically spaced wave numbers can span an overall range of more than $2000\ \mathrm{cm}^{-1}$, resulting in a measurement of t to an accuracy of about 1 part in 10^7, limited by the Michelson wavelength meter.

[1] R. Castell, W. Demtröder, A. Fischer, R. Kullmer, H. Weickenmeier, and K. Wickert, Appl. Phys. B: Photophys. Laser Chem. **38**, 1 (1985).
[2] K. W. Meissner, J. Opt. Soc. Am. **31**, 405 (1941).
[3] B. W. Petley, K. Morris, and R. E. Shawyer, J. Phys. B **13**, 3099 (1980).
[4] S. R. Amin, C. D. Caldwell, and W. Lichten, Phys. Rev. Lett. **47**, 1234 (1981).
[5] C. J. Sansonetti, in *Advances in Laser Science IV*, edited by J. L. Gole *et al.* (American Institute of Physics, NY, 1988), p. 548.
[6] C. J. Sansonetti, J. D. Gillaspy, and C. L. Cromer, Phys. Rev. Lett. **65**, 2539 (1990).
[7] J. D. Gillaspy and C. J. Sansonetti, J. Opt. Soc. Am. B **8**, 2414 (1991).
[8] J. R. Benoit, J. Phys. Radium **7**, 57 (1898).
[9] W. H. J. Childs, J. Sci. Instrum. **3**, 97 (1926).
[10] H. Buisson and Ch. Fabry, J. Phys. (Paris)0302-072X **7**, 169 (1908).
[11] J. M. Bennett, J. Opt. Soc. Am. **54**, 612 (1964).
[12] A. Harasaki, J. Schmit, and J. C. Wyant, Appl. Opt. **40**, 2102 (2001).
[13] M. S. Sorem and A. L. Schawlow, Opt. Commun. **5**, 148 (1972).
[14] R. E. Machol and E. R. Westrum, Jr., J. Am. Chem. Soc. **80**, 2950 (1958).
[15] J. L. Hall and S. A. Lee, Appl. Phys. Lett. **29**, 367 (1976).
[16] D. H. McIntyre and T. W. Hänsch, Phys. Rev. A **34**, 4504 (1986).
[17] D. H. McIntyre and T. W. Hänsch, Phys. Rev. A **36**, 4115 (1987).
[18] D. H. McIntyre, W. M. Fairbank, Jr., S. A. Lee, T. W. Hänsch, and E. Riis, Phys. Rev. A **41**, 4632 (1990).
[19] G. P. Barwood, W. R. C. Rowley, P. Gill, J. L. Flowers, and B. W. Petley, Phys. Rev. A **43**, 4783 (1991).